De Novo Variants in *MAPK8IP3* Cause Intellectual Disability with Variable Brain Anomalies

Konrad Platzer,[1,*] Heinrich Sticht,[2] Stacey L. Edwards,[3] William Allen,[4] Kaitlin M. Angione,[5] Maria T. Bonati,[6] Campbell Brasington,[7] Megan T. Cho,[8] Laurie A. Demmer,[7] Tzipora Falik-Zaccai,[9,10] Candace N. Gamble,[11] Yorck Hellenbroich,[12] Maria Iascone,[13] Fernando Kok,[14] Sonal Mahida,[15] Hanna Mandel,[9] Thorsten Marquardt,[16] Kirsty McWalter,[8] Bianca Panis,[17] Alexander Pepler,[18] Hailey Pinz,[19] Luiza Ramos,[14] Deepali N. Shinde,[20] Constance Smith-Hicks,[15] Alexander P.A. Stegmann,[21] Petra Stöbe,[18] Constance T.R.M. Stumpel,[21] Carolyn Wilson,[4] Johannes R. Lemke,[1] Nataliya Di Donato,[22] Kenneth G. Miller,[3,23] and Rami Jamra[1,23]

Using exome sequencing, we have identified *de novo* variants in *MAPK8IP3* in 13 unrelated individuals presenting with an overlapping phenotype of mild to severe intellectual disability. The *de novo* variants comprise six missense variants, three of which are recurrent, and three truncating variants. Brain anomalies such as perisylvian polymicrogyria, cerebral or cerebellar atrophy, and hypoplasia of the corpus callosum were consistent among individuals harboring recurrent *de novo* missense variants. *MAPK8IP3* has been shown to be involved in the retrograde axonal-transport machinery, but many of its specific functions are yet to be elucidated. Using the CRISPR-Cas9 system to target six conserved amino acid positions in *Caenorhabditis elegans*, we found that two of the six investigated human alterations led to a significantly elevated density of axonal lysosomes, and five variants were associated with adverse locomotion. Reverse-engineering normalized the observed adverse effects back to wild-type levels. Combining genetic, phenotypic, and functional findings, as well as the significant enrichment of *de novo* variants in *MAPK8IP3* within our total cohort of 27,232 individuals who underwent exome sequencing, we implicate *de novo* variants in *MAPK8IP3* as a cause of a neurodevelopmental disorder with intellectual disability and variable brain anomalies.

Introduction

The prevalence of intellectual disability (ID) in the general population is estimated to be around 1% and has become the most frequent reason for referral to pediatric genetic services.[1,2] Genetically, ID is extremely heterogeneous, and *de novo* variants detected via trio exome sequencing are the major etiology in children of unrelated parents.[3,4] Disease-related genes of developmental delay (DD) or ID can be identified through the widespread use of next-generation-sequencing followed by collaborative efforts and the use of matchmaking platforms to prove causation through accumulating a sufficient number of individuals with overlapping phenotypes and *de novo* variants in the same gene, as well as through functional analyses in model organisms. After the initial identification of a *de novo* missense variant in *MAPK8IP3* (MIM 605431) in an individual with ID, the gene became an appealing candidate for further investigation in light of the established role that MAPK8IP3 orthologs play in axonal transport in vertebrates and invertebrates.[5] In addition, three *de novo* variants had been separately published in individuals with a neurodevelopmental disorder.[4,6,7] Through international collaboration, we identified 13 individuals with DD and/or ID who harbor heterozygous *de novo* variants in *MAPK8IP3*. Through *in silico* molecular modeling and functional analyses in *Caenorhabditis elegans*, we provide further evidence for pathogenicity and causality, as well as primary insights into the specific role of certain domains in MAPK8IP3's diverse functions.

Material and Methods

Study Subjects

This study was approved by the ethics committee of the University of Leipzig (approval code: 402/16-ek). Through matchmaking[8] and

[1]Institute of Human Genetics, University of Leipzig Hospitals and Clinics, Leipzig 04103, Germany; [2]Institute of Biochemistry, Emil-Fischer Center, Friedrich-Alexander-Universität Erlangen-Nürnberg, Erlangen 91054, Germany; [3]Genetic Models of Disease Laboratory, Oklahoma Medical Research Foundation, Oklahoma City, OK 73104, USA; [4]Department of Genetics, Fullerton Genetics Center, Asheville, NC 28803, USA; [5]Department of Pediatrics, Section of Clinical Genetics and Metabolism, University of Colorado School of Medicine, Aurora, CO 80045, USA; [6]Clinic of Medical Genetics, IRCCS Istituto Auxologico Italiano, Milan 20149, Italy; [7]Department of Pediatrics, Clinical Genetics, Levine Children's Hospital at Carolina Healthcare System, Charlotte, NC 28203, USA; [8]GeneDx, Gaithersburg, MD 20877, USA; [9]Institute of Human Genetics, Galilee Medical Center, Nahariya 22100, Israel; [10]The Azrieli School of Medicine, Bar-Ilan University, Safed 1311502, Israel; [11]Department of Pediatrics, University of Texas Health Medical School, Houston, TX 77030, USA; [12]Institute of Human Genetics, University of Lübeck, Lübeck 23562, Germany; [13]Laboratorio di Genetica Medica, Azienda Socio Sanitaria Territoriale Papa Giovanni XXIII, Bergamo 24127, Italy; [14]Mendelics Genomic Analysis, São Paulo 04013-000, Brazil; [15]Department of Neurology, Kennedy Krieger Institute, the Johns Hopkins University School of Medicine, Baltimore, MD 21205, USA; [16]Department of Pediatrics, University Hospital Münster, Münster 48149, Germany; [17]Department of Pediatrics, Zuyderland Medical Center, Heerlen and Sittard 6419, the Netherlands; [18]CeGaT GmbH and Praxis für Humangenetik Tübingen, Tübingen 72076, Germany; [19]Division of Medical Genetics, Department of Pediatrics, Saint Louis University School of Medicine, Saint Louis, MO 63104, USA; [20]Division of Clinical Genomics, Ambry Genetics, Aliso Viejo, CA 92656, USA; [21]Department of Clinical Genetics and School for Oncology and Developmental Biology, Maastricht University Medical Center, Maastricht 6229, the Netherlands; [22]Institute for Clinical Genetics, Carl Gustav Carus Faculty of Medicine, TU Dresden, Dresden 01307, Germany
[23]These authors contributed equally to this work
*Correspondence: konrad.platzer@medizin.uni-leipzig.de
https://doi.org/10.1016/j.ajhg.2018.12.008.

international collaborative efforts, we identified 13 individuals who harbored heterozygous *de novo* variants in *MAPK8IP3* and had an overlapping phenotype of DD and/or ID; these individuals were referred from different centers in Brazil, Germany, Israel, Italy, the USA, and the Netherlands. Referring physicians provided detailed clinical information via a uniform clinical questionnaire. Informed consent was obtained from all examined individuals or their legal guardians. In some cases, testing was done as part of routine clinical care and therefore institutional ethics approval was not required. If done in a research setting, the testing was approved by the ethics committees of the respective centers. All families provided informed consent for clinical testing and publication.

Identification and Evaluation of Variants

Exome sequencing via standard commercial products was performed within diagnostic or research settings in a total cohort of 27,232 affected individuals (Supplemental Material and Methods). Candidate variants were prioritized on the basis of gene and variant attributes, minor-allele frequency, effect on protein function, status determined by *in silico* prediction tools, phenotype, family history, and inheritance according to the local proceedings in the respective centers. Individuals 1 and 4 were identified in a cohort of 5,926 individuals with neurodevelopmental disorders (NDDs); individual 2 was identified in a cohort of 4,600 individuals with a variety of clinical indications; individuals 3, 6, 9, 10, and 12 were identified in a cohort of 14,113 individuals with NDD; individuals 5 and 8 were identified in a cohort of 393 individuals with NDD; individual 7 was identified in a cohort of 200 individuals with NDD; individual 11 was identified in a cohort of 1,400 individuals with NDD; and individual 13 was identified in a cohort of 600 individuals with NDD. *De novo* occurrence was confirmed in all individuals. The families of all individuals, except for individual 2, underwent trio exome sequencing. The *de novo* nonsense variant in individual 2 was identified by single-exome sequencing and a subsequent search for truncating variants among highly constrained genes with a probability of loss-of-function intolerance score (pLI-score) >0.95.[9] The *de novo* occurrence was confirmed with Sanger sequencing. The Exome Aggregation Consortium (ExAC) database and the Genome Aggregation Database (gnomAD) served as control populations.[9]

Statistical Analysis for Enrichment of *De Novo* Variants in *MAPK8IP3*

The statistical analysis was done with R. We used a binomial test and an established framework of gene-specific mutation rates[10] to test whether the occurrence of the number of *de novo* variants in *MAPK8IP3* in our cohort was significantly greater than would be expected by chance.

Structural Modeling

Structural analysis of the variants p.Leu444Pro and p.Glu461Gly[7] was performed on the basis of the known crystal structures of the leucine zipper domain of murine MAPK8IP3 (PDB: 6EJN[11]), which exhibits 99% sequence identity to human MAPK8IP3. We modeled the structure of the MAPK8IP3 WD40 repeat that harbors the variants p.His994Gln and p.Arg1146Cys by using the homologous domain from Ciao1 (PDB: 3FM0[12]) as a template. For the remaining variants, modeling was not possible because of the lack of suitable template structures. Amino acid exchanges were modeled with SwissModel,[13] and structure visualization was performed with RasMol.[14] All sequence positions reported for the structures were adjusted to match those of the MAPK8IP3 isoform investigated in the present study.

Caenorhabditis elegans Functional Analyses

De novo variants in *MAPK8IP3* have so far been reported on three separate occasions in three individuals with neurodevelopmental disorders. The reported variants are c.281A>G (p.Tyr94Cys),[6] c.1382A>G (p.Glu461Gly),[7] and c.3436C>T (p.Arg1146Cys).[4] These three variants from the literature and the variants in our cohort (the missense variants c.1331T>C [p.Leu444Pro] and c.1574G>A [p.Arg525Gln] and the truncating variant c.111C>G [p.Tyr37*]) affect amino acid positions that are conserved up to *C. elegans,* enabling us to perform functional analyses (Figure 3A). In *C. elegans*, the MAPK8IP3 ortholog is known as UNC-16, which is encoded by the *unc-16* gene. *C. elegans unc-16* loss-of-function mutations are recessive and are associated with sluggish locomotion and impaired clearance of organelles from axons.[15–17] In mutants lacking UNC-16, axonal transport is disrupted such that a subset of cell soma organelles, including lysosomes, early endosomes, and Golgi, aberrantly enter axons and accumulate in the synaptic region. This function of UNC-16 is conserved in mammals; as an example, mouse neurons lacking MAPK8IP3 (known as JIP3 in mammals) accumulate lysosomes in their axons.[18]

To determine the extent to which these six variants disrupt the function of UNC-16, we used CRISPR genome editing to engineer the six variants onto the native *C. elegans unc-16* gene. Then we assayed the six mutant strains for locomotion function and lysosome accumulation in the axons. We then compared the strains to wild-type and an *unc-16* reference null mutant.[15] To control for off-target effects, we again used CRISPR genome editing to reverse-engineer each mutant allele back to its wild-type sequence; this produced "rescued" alleles, which were subjected to the same assays.

To visualize individual lysosomes in neurons, we crossed mutants with a genomically integrated transgene that expresses fluorescently tagged lysosomes in a set of nine ventral cord cholinergic motor neurons. We then counted lysosomal puncta exceeding a pre-defined threshold.[15,17]

Placing *C. elegans* in liquid over a smooth agar surface induces an escape response in which the animal alters its locomotion pattern and attempts to escape the liquid via high frequency swimming. For each strain, we counted swimming cycles in 72 animals for 3 min per animal and obtained averages. At 23° C, wild-type has ~100 swimming cycles per min (i.e., over 20,000 cycles for the 72 animals). To assay locomotion function in the mutants, we quantified the rate of swimming cycles. We performed swimming-cycle assays by using a modification of the originally described "thrashing assay."[19] When counting swimming cycles, we focused on one side of the animal in the middle of the body and counted each time that part went through a complete cycle. We started the timer when the animal was beginning the cycle, such that the first count represents one complete cycle (for further details on *C. elegans* functional analyses, see Supplemental Material and Methods).

Results

Clinical Description

An overview of the main clinical symptoms of 13 individuals harboring *de novo* variants in *MAPK8IP3* is presented in Table 1 (see Table S1 for detailed phenotypic

Table 1. Summary of Clinical Features of Individuals with Causative *De Novo* Variants in *MAPK8IP3*.

Individual	*De Novo* Variant	p.	Sex	Age	DD and ID (IQ)	ASD	Sz	Neurological Exam	Microcephaly	Brain Anomalies	Other
1	c.65delG	p.(Gly22Ala*fs**3)	M	14 yr	moderate (48)	+	–	MH, ataxia	–	cerebellar atrophy, white-matter hyperintensity in posterior limbs of internal capsules	scoliosis
2	c.79G>T	p.(Glu27*)	M	4 yr	severe	–	–	MH, ataxia	–	no	–
3	c.111C>G	p.(Tyr37*)	M	4 yr	moderate	–	–	MH	–	no	–
4	c.1198G>A	p.(Gly400Arg)	M	7 yr	mild	+	–	–	–	NA	–
5	c.1331T>C	p.(Leu444Pro)	M	10 yr	moderate (49)	–	1× gSz	MH	–	perisylvian polymicrogyria	scoliosis
6			F	9 yr	mild	–	–	MH	–	perisylvian polymicrogyria	–
7	c.1574G>A	p.(Arg525Gln)	F	3 yr	mild	–	–	–	−2.7 SD.	no	–
8	c.1732C>T	p.(Arg578Cys)	F	5 yr	severe	–	1× gSz	MH, SP	−2.5 SD.	cerebral atrophy, white-matter volume loss, thin CC with hypoplasia of rostrum and splenium, cerebellar atrophy	short stature
9			F	6 yr	moderate	–	1× gSz	MH, SP	−2.5 SD.	cerebral atrophy, white-matter volume loss, thin CC, cerebellar hypoplasia predominant in inferior vermis	short stature
10	c.2982C>G	p.(His994Gln)	M	4 yr	moderate	–	gSz	MH	–	no	–
11	c.3436C>T	p.(Arg1146Cys)	F	11 yr	mild	–	–	SP	–	mild cerebral atrophy, white-matter volume loss, thin CC	cortical visual impairment
12			F	4 yr	severe	–	–	SP	–	short CC	–
13			F	19 yr	moderate (49)	–	–	MH, unstable gait	–	white-matter volume loss, thin CC	cortical visual impairment, scoliosis

Variant nomenclature corresponds to GenBank: NM_015133.4. Abbreviations are as follows: ASD = autism spectrum disorder; CC =corpus callosum; DD = developmental delay; ID = intellectual disability; F = female; M = male; MH = muscular hypotonia; NA = not available; SP = spasticity; and gSz = generalized seizures. Further clinical details are provided in Table S1.

descriptions). The onset of symptoms was noted in infancy or early childhood; all 13 individuals displayed DD and a variable degree of ID between mild (4/13; 31%), moderate (6/13; 46%), and severe (3/13; 23%). Furthermore, two individuals were diagnosed with an autism spectrum disorder (ASD). 11 individuals showed abnormalities of muscular tone (hypotonia in nine and spasticity in four; two individuals showed both). Two individuals presented with signs of ataxia, and one presented with an unstable gait. In addition, two individuals had cortical visual impairment, and three individuals had scoliosis. Growth development of individuals in our cohort was mostly normal, although short stature in two and microcephaly of −2.5, −2.5, and −2.7 standard deviations in three individuals were exceptions. One individual had recurrent generalized seizures, and three individuals had events involving one generalized seizure only. None of the individuals was reported to show signs of developmental regression, and there was no consistent finding of facial dysmorphism.

Brain Imaging

Cranial MRI was performed for all individuals, apart from individual 4. The MRIs of four individuals (individuals 2, 3, 7 and 10) were reported to be unremarkable. The cranial MRIs of all remaining individuals (individuals 1, 5, 6, 8, 9, 11, 12, and 13) were evaluated for this study and showed a variety of brain anomalies affecting both cerebral and cerebellar structures (Figure 1). Two individuals presented with bilateral perisylvian polymicrogyria with otherwise normal brain structures. One individual showed mild cerebellar atrophy and white-matter hyperintensity in the posterior limbs of the internal capsules. A very thin or short corpus callosum was noted in five individuals, three of whom also showed signs of cerebral atrophy, and four of whom presented with considerable white-matter volume loss.

Causative Variants

By using exome sequencing, we identified *de novo* protein-affecting, single-nucleotide variants in *MAPK8IP3* in 13 individuals (Figure 2A). All identified variants were absent from gnomAD. All three of the truncating variants are located in the first exon of *MAPK8IP3*; thus, nonsense-mediated mRNA decay is likely.[20] The six missense variants, three of which are recurrent, affect amino acids that are highly conserved up to zebrafish, or even further, and all are predicted to be deleterious by multiple *in-silico* prediction programs (Table S2). According to data from ExAC, *MAPK8IP3* is a gene with a significantly reduced number of truncating and missense variants in controls, indicating a selective constraint on both types of variants in a control population that lacks severe, early-onset phenotypes such as DD and ID (pLI score = 1.00; z score for missense variants = 4.06).[9]

Enrichment of *De Novo* Variants in *MAPK8IP3* in 27,232 Individuals

Altogether, we performed exome sequencing in 27,232 individuals, a majority of whom had been diagnosed with a neurodevelopmental disorder. Because the estimated probability of mutation (missense, nonsense, frameshift) for *MAPK8IP3* is roughly 0.629×10^{-4},[10] the occurrence of 13 *de novo* variants is highly unlikely to have occurred by chance ($p = 6.165\times10^{-5}$). This is probably a conservative estimate; the *de novo* nonsense variant in individual 2 was identified through single-exome sequencing in a cohort of 4,600 individuals with a variety of clinical indications and a subsequent segregation analysis of only truncating variants in genes with a pLI > 0.95.[9]

In Silico Structural Modeling

A structural analysis of MAPK8IP3 indicates that the variant-affected amino acid positions Leu444 and Glu461 are located in the leucine zipper domain, which forms a homodimeric structure consisting of two α helices oriented in a parallel fashion. Leu444 is located immediately adjacent to the binding site of the KLC2 tetratricopeptide (TPR) domain (Figure 2B). A closer inspection of the zipper structure reveals that the Leu444 side chains from both subunits form contacts with each other (Figure 2C), but these contacts are absent in the p.Leu444Pro variant (Figure 2D). In addition, proline is known to act as a strong α helix breaker, and thus this exchange is expected to severely affect both the structure of the helical subunits and the homodimer formation and, consequently, the interaction with TPR-domains.

In contrast, the structural effect of the p.Glu461Gly[7] variant appears to be less severe. The Glu461 side chain forms weak electrostatic interactions with Lys466; these interactions are absent in the p.Glu461Gly variant (Figures 2E and 2F). In addition, p.Glu461Gly might have a negative effect on helix stability because of enhanced backbone flexibility.

Inspection of the WD40-domain model indicates that His994 and Arg1146 are oriented toward the solvent and do not form significant interactions with other residues of the domain. This observation, together with the high sequence-conservation among orthologs, might indicate that the respective residues play a role for protein-protein interactions rather than for WD40-domain stability. WD40 domains are a large group of protein-interaction domains, which recognize protein ligands via divergent surface patches.[21]

Axonal Lysosomal Density in *C. elegans*

The MAPK8IP3 mutant corresponding to p.Tyr37* had an axonal lysosomal density about 88-fold higher than that of wild-type (Figures 3B and 3C). This was slightly greater than that of the reference null mutant, which corresponds to p.Asn316* in MAPK8IP3. The p.Tyr37* mutant phenotype was entirely caused by the disrupted function of UNC-16: reverse engineering the sequence back to the wild-type sequence corrected the lysosomal density to the wild-type density (Figure 3C). In addition to modeling

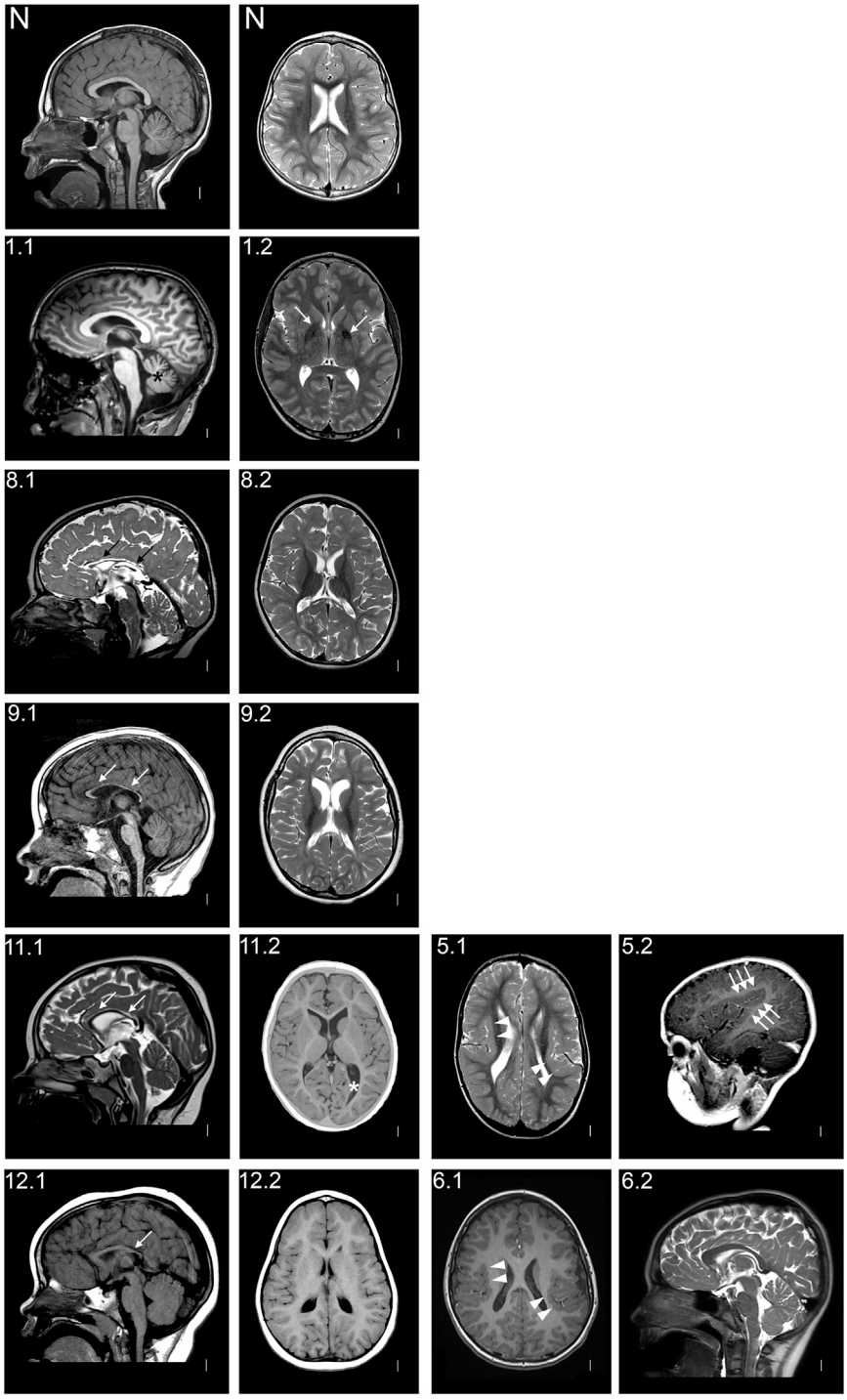

Figure 1. MRI of Individuals with Brain Anomalies

Images of affected individuals are labeled with numbers as listed in Table 1, and there are two images for each individual. N represents a T1 sagittal midline (left) and a T2 axial (right) image of a healthy individual.

(1.1 and 1.2) T1 midline sagittal and T2 axial images taken at the age of 10 years show mild cerebellar vermis hypoplasia (black asterisk) and hyperintensity in the posterior limbs of the internal capsules (white arrows).

(8.1 and 8.2) T2 midline sagittal and axial images taken at the age of 3 years demonstrate very thin corpus callosum with hypoplasia of the rostrum and splenium (black arrows), cerebral atrophy with broad sulci, and reduced white-matter volume and cerebellar atrophy.

(9.1 and 9.2) T1 midline sagittal and T2 axial images taken at the age of 5 years show a thin corpus callosum (white arrows) and cerebellar and cerebral atrophy with white-matter volume loss.

(11.1 and 11.2) T2 midline sagittal and T1 IR axial images taken at the age of 3 years show a thin corpus callosum (white arrows) and mild cerebral atrophy with white-matter volume loss, predominantly in the occipital lobes, as well as enlarged lateral ventricles (white asterisk).

(12.1 and 12.2) T1 midline sagittal and axial images taken at the age of 26 months demonstrate short and thin corpus callosum but otherwise normal morphology.

(5.1 and 5.2) T2 axial image and a T1 sagittal image (viewed through the right sylvian fissure) taken at the age of 3 years show bilateral perisylvian polymicrogyria (arrow heads and triple arrows).

(6.1 and 6.2) T1 axial and T2 midline sagittal images taken at the age of 8 years show bilateral perisylvian polymicrogyria (white arrowheads) with otherwise unremarkable midline structures.

the nonsense variant, we engineered five missense mutants, but the remaining three variants were not conserved in *C. elegans* and were thus not included. Of the five missense mutants, only that corresponding to p.Leu444Pro had a significantly elevated axonal lysosome density (~15-fold higher than that of wild-type; Figures 3B and 3C). Reverse engineering the proline 444 back to leucine corrected the axonal lysosome density to a level not significantly different from that of the wild-type (Figure 3C). The remaining four variants produced non-significant results.

Locomotion Assay in *C. elegans*

The *unc-16* reference null mutant had a swimming-cycle rate that was ~35% of the wild-type rate (Figure 3D). Overall, five of the six investigated mutants had swimming-cycle rates that were significantly lower than their reverse-engineered counterparts. The mutant corresponding to MAPK8IP3 p.Tyr37* had a swimming rate similar to that of the reference null mutant (Figure 3D). The mutant corresponding to MAPK8IP3 p.Leu444Pro had a swimming rate that was ~50% of the wild-type rate and only 55% higher than that of the reference null mutant, again indicating a strong loss of function for this mutant (Figure 3D). Three of the other mutants had swimming rates that were 93%–94% of their reverse-engineered counterparts, but this was still

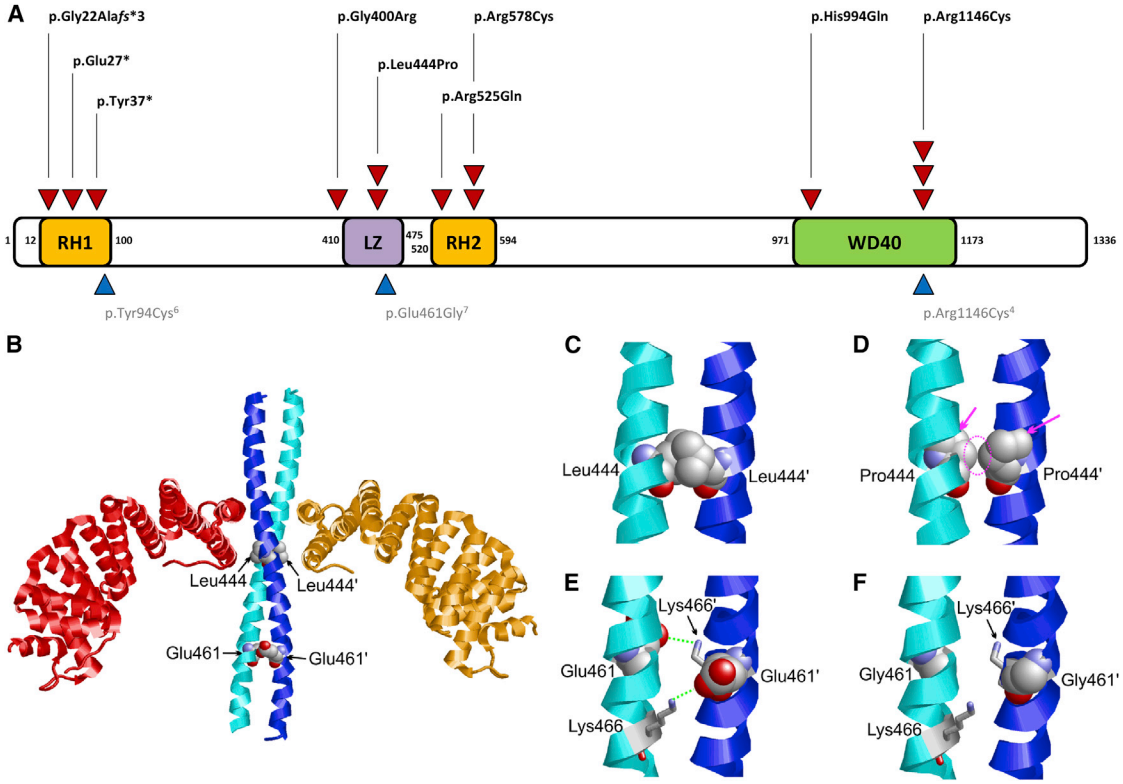

Figure 2. ***De Novo*** **Variants in MAPK8IP3 and Structural Effects in the Leucine Zipper Domain**
(A) Location of *de novo* single-nucleotide variants in MAPK8IP3 with respect to domain structure (GenBank: NM_015133.4). Red triangles = individuals from this cohort. Blue triangles = published variants in individuals with a neurodevelopmental disorder. Abbreviations are as follows: LZ =leucine zipper; RH1 and RH2 = Rab-interacting lysosomal protein (RILP) homology 1 and 2.
(B) Crystal structure of the MAPK8IP3 leucine zipper (cyan and blue) in complex with two TPR domains of the kinesin light chain (orange and red). The sites of the sequence variants detected in the present study are shown in space-filled presentation.
(C) The Leu444 sidechains of the homodimeric leucine zipper interact with each other (a prime denotes residues of the second subunit).
(D) In the p.Leu444Pro variant, these interactions are lost as a result of the shorter proline sidechain (dotted circle). In addition, the cyclic proline sidechain causes a steric clash with the backbone of adjacent helix residues (magenta arrows). Both effects are expected to cause a drastic destabilization of the helix and to impede homodimer formation.
(E) The Glu461 side chain forms weak inter-subunit electrostatic interactions with Lys466 (green dotted lines).
(F) The p.Glu461Gly variant cannot form these polar interactions because there is no charged sidechain.

highly significant because of the large sample size and large number of swimming cycles counted for each strain (Figure 3D). The mutants with milder, but statistically significant, locomotion phenotypes correspond to MAPK8IP3 p.Tyr94Cys, p.Arg525Gln, and p.Glu461Gly. The remaining mutant, corresponding to p.Arg1146Cys, showed non-significant results.

Discussion

In this study, we describe in detail 13 individuals with intellectual disability and variable brain anomalies. All individuals harbor *de novo* truncating or missense variants in *MAPK8IP3;* this represents a significant statistical enrichment within our cohort in light of the fact that this gene is under constraint of such variants. To further underscore pathogenicity, we modeled adverse structural effects of variants located in the leucine zipper domain, and we functionally characterized a subset of variants in *C. elegans* showing increased lysosomal density and abnormal locomotion. Thus, taking all lines of evidence together, we firmly establish *de novo* variants in *MAPK8IP3* as a cause of developmental delay and/or intellectual disability with variable brain anomalies such as perisylvian polymicrogyria, as well as cerebral and cerebellar atrophy.

MAPK8IP3 has been shown to be part of the axonal transport machinery, which is essential for the function and maintenance of neurons.[5] It supplies the synapse with newly synthesized proteins and lipids while damaged or misfolded proteins are cleared. Defects in axonal transport can lead to progressive neuronal cell death[22] and have initially been associated with a wide range of neurodegenerative diseases, for example hereditary spastic paraplegia, Parkinson disease, Alzheimer disease, and other forms of dementia.[23] But certain components of the axonal transport machinery, such as the dynein heavy chain 1 (DYNC1H1) and BICD2 have also been implicated in childhood-onset neurodevelopmental disorders comprising ID and a spectrum of malformations of

A

Pair number	Mutant	Rescue	*C. elegans* variant	Human variant
1	unc-16(ce483) null	wild-type	p.Gln304*	p.Asn316*
2	unc-16(ce857)	unc-16(ce858)	p.Tyr49*	p.Tyr37*
3	unc-16(ce853)	unc-16(ce859)	p.Tyr106Cys	p.Tyr94Cys
4	unc-16(ce856)	unc-16(ce863)	p.Leu393Pro	p.Leu444Pro
5	unc-16(ce852)	unc-16(ce862)	p.Glu411Gly	p.Glu461Gly
6	unc-16(ce854)	unc-16(ce860)	p.Arg461Gln	p.Arg525Gln
7	unc-16(ce851)	unc-16(ce861)	p.Arg1028Cys	p.Arg1146Cys

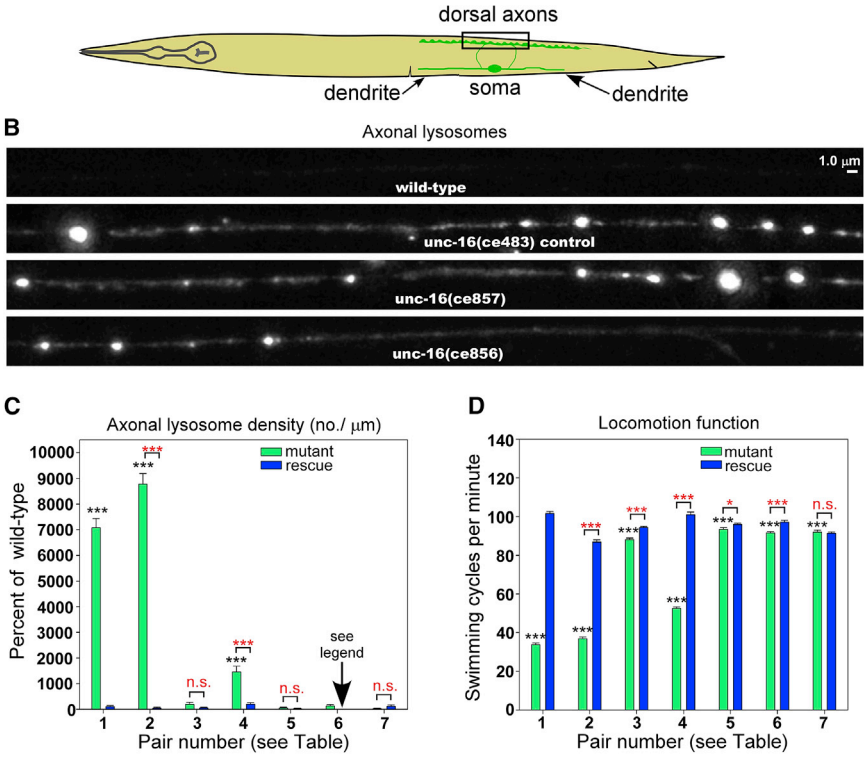

Figure 3. Impact of Variants on Axonal Lysosome Density and Locomotion

(A) List of all *C. elegans unc-16* mutations produced in the study, along with their corresponding wild-type revertants. "Pair number" refers to numbers on the X axes of the graphs. "Rescue" means that the mutation has been reverted to the wild-type amino acid sequence. The amino acid positions of each mutation on the UNC-16 protein in *C. elegans* and MAPK8IP3 in *H. sapiens* (GenBank: NM_015133.4) are indicated.

(B and C) Representative images and quantification of lysosome density in DB6 and DA6 motor neuron axons in the indicated genotypes. The rectangle in the drawing indicates the imaged region. The lysosome marker CTNS-1-RFP is expressed from the integrated transgene *ceIs56*. Representative images were chosen on the basis of density per µm and are identically scaled. Graph data depict lysosome number per µm of axon length exceeding a threshold intensity and are means and standard errors (SEMs) from 57–68 animals each. No rescue data were obtained for "6" because it was not significantly different from the wild-type. Black asterisks compare the marked bar to the wild-type value. Red asterisks compare the indicated two bars in a group. Unmarked bars are not significantly different from the wild-type or the other bar in the group. *** indicates p values that are < 0.001. n.s. = not significant.

(D) Swimming cycles per min for the indicated genotypes. Data are means and SEMs from 72 animals for each strain. Black asterisks compare the marked bar to the wild-type value. Red asterisks compare the indicated two bars in a group. * and *** indicate $p < 0.05$ or < 0.001, respectively. n.s. = not significant.

cortical development (MCD), such as lissencephaly and (bilateral perisylvian) polymicrogyria.[24–27] In addition, the disruption of proteins (such as CDK5[17] and NTRK2[28] [alternative name TRKB]) that directly interact with MAPK8IP3 has been shown to cause childhood-onset phenotypes of ID, lissencephaly, and cerebellar hypoplasia.[29–32] Taken together, these overlapping phenotypic effects of ID and variable brain anomalies due to the disruption of other parts of the axonal transport machinery provide another line of evidence for the causal role of *MAPK8IP3* in the genesis of ID and variable brain anomalies.

Although our observations are based on a small cohort of 13 individuals, we observe several hints for genotype-phenotype correlations, which are especially striking with respect to brain anomalies in individuals harboring recurrent missense variants: (1) both individuals with the missense variant p.Leu444Pro presented with a very similar bilateral perisylvian polymicrogyria (PMG) with otherwise normal brain structures; (2) both individuals with the missense variant p.Arg578Cys presented with an overlapping phenotype of cerebral atrophy, considerable white-matter volume loss, and a very thin corpus callosum, as well as cerebellar atrophy or hypoplasia; and (3) two of three individuals with the missense variant p.Arg1146Cys showed white-matter volume loss and a thin corpus callosum. In comparison, the third individual with the p.Arg1146Cys variant showed a short corpus callosum only. This mostly consistent overlap of brain anomalies in individuals with recurrent *de novo* missense variants could suggest variant-specific functional consequences possibly related to MAPK8IP3's domain constitution. Further studies with additional individuals harboring the same *de novo* variants will have to investigate whether these preliminary observations can be confirmed in a bigger cohort. Other aspects of a possible genotype-phenotype correlation include signs of an ataxic gait in two of three individuals with truncating variants; spasticity, short stature, and microcephaly in both individuals harboring the variant p.Arg578Cys; and the occurrence of spasticity and cortical visual impairment in two individuals with the p.Arg1146Cys variant. Although these phenotypic presentations recurred within our cohort, there is only

very limited evidence that seizures are truly part of the phenotypic spectrum of *MAPK8IP3*-related neurodevelopment disorders: three individuals had only one event of a generalized seizure each, and two of these occurred during febrile episodes; and individual 10, who had recurrent generalized seizures, in fact harbors a second *de novo* missense variant in *SLC6A1* (MIM: 137165), a gene associated with myotonic-atonic epilepsy (see Table S1). This could be a rare case of an individual in whom two monogenic disorders both cause an NDD phenotype.

PMG constitutes an MCD with a plethora of non-genetic causes, such as congenital infections and hypoxia, in contrast to a wide range of monogenic causes.[33] The most common location for PMG is the perisylvian region.[34] PMG is poorly understood in regard to its origin in brain development, and the term "polymicrogyria" has been used imprecisely in the literature.[35] Presently, PMG in humans is not thought to arise because of disrupted migration of cortical neurons; instead it more likely represents a postmigration disorder involving the fusion of cortical laminae.[35,36] In a recent study,[37] *MAPK8IP3*'s mediation of NTRK2 axonal anterograde transport implicated it in the regulation of radial migration, and the expression of MAPK8IP3 was shown to gradually increase from embryonic day 10 to postnatal day 10; especially elevated periods occurred at the time of migration.

De novo variants in *MAPK8IP3* have so far been independently reported in three individuals with an NDD. Only one detailed phenotypic description is available: that of a ten-year-old female with a tentative clinical suspicion of Smith-Magenis-Syndrome.[7] The girl showed moderate ID and muscular hypotonia fitting the spectrum of *MAPK8IP3*-related neurodevelopmental disorders described in our cohort. The other two reported *de novo* missense variants comprise (1) a variant found in the context of the Deciphering Developmental Delay study,[4] c.3436C>T (p.Arg1146Cys), which we also identified in three individuals in our cohort, and (2) c.281A>G (p.Tyr94Cys) in an individual with autistic features.[6] Interestingly, the latter *de novo* variant was identified in a male individual with an IQ > 90. Nonetheless, combined with the observation of autistic features in two individuals in our cohort, this strengthens the possibility that ASD is part of the spectrum of *MAPK8IP3*-related neurodevelopmental disorders. ID and ASD show a significant molecular overlap. However, it is unclear whether this overlap is due to shared molecular pathways between two distinct neurodevelopmental disorders or whether it represents two aspects of clinical presentation within a certain genetic disorder.[2,38]

The truncating variants p.Tyr37* and p.Leu444Pro constitute the variants displaying the most drastic changes in the model and functional assays we studied, but the intellectual outcome was in fact more severe in other individuals. Four of the six missense variants had relatively mild functional consequences with respect to axonal lysosome accumulation and locomotion, and the variant p.Arg1146Cys showed only non-significant alterations despite constituting the most recurrent *de novo* variant (seen in four individuals overall). This is not surprising because MAPK8IP3 is a large protein and appears to have evolved at least two independent functions that are distinguished by different cargos and interactions with different motors.[5] One function, assayed in this study, is the organelle clearance function, which appears to be conserved from *C. elegans* to mammals[15,18] and functions independently of the Kinesin-1 motor.[5,15] However, MAPK8IP3 also has a Kinesin-1-dependent adaptor function that appears to connect the Kinesin-1 motor to Kinesin-1 cargoes that are carried on or within small transport vesicles.[5] So far, the only MAPK8IP3 adaptor cargo that has been clearly defined is NTRK2,[28,39] which is a receptor for brain-derived neurotrophic factor (BDNF) that has no homologs in *C. elegans*. Other studies have found that MAPK8IP3's Kinesin-1-dependent function(s) are important for axonal elongation.[40–42] One of these studies provided evidence that MAPK8IP3 itself was the relevant Kinesin-1 cargo for axonal elongation and found that MAPK8IP3 had a stimulatory effect at growing axon tips.[40] In *C. elegans* there are no assays for the Kinesin–dependent functions of MAPK8IP3, and there is no evidence for axonal elongation defects in *C. elegans* mutants lacking MAPK8IP3. We hypothesize that the four variants with no detectable organelle-clearance defects disrupt protein domains that are not required for organelle clearance but that are required for one or more of MAPK8IP3's functions, such as Kinesin-1-dependent axonal development.

In summary, we establish *de novo* variants in *MAPK8IP3* as a cause of ID and variable brain anomalies, further implicating defects in the axonal transport machinery in neurodevelopmental disorders.

Supplemental Data

Supplemental Data include Supplemental Material and Methods and two tables and can be found with this article online at https://doi.org/10.1016/j.ajhg.2018.12.008.

Acknowledgments

We thank the families for their participation and support of this study. We thank Kelly Schoch for providing clinical follow-up information on one individual.

Declaration of Interests

The authors declare no competing interests.

Received: November 2, 2018
Accepted: December 11, 2018
Published: January 3, 2019

Web Resources

DECIPHER, https://decipher.sanger.ac.uk/
ExAC Browser, http://exac.broadinstitute.org/

GenBank, https://www.ncbi.nlm.nih.gov/genbank/
GeneMatcher, https://genematcher.org/
GnomAD, http://gnomad.broadinstitute.org/
OMIM, http://www.omim.org/
R, http://www.r-project.org/

References

1. Maulik, P.K., Mascarenhas, M.N., Mathers, C.D., Dua, T., and Saxena, S. (2011). Prevalence of intellectual disability: A meta-analysis of population-based studies. Res. Dev. Disabil. *32*, 419–436.
2. Vissers, L.E.L.M., Gilissen, C., and Veltman, J.A. (2016). Genetic studies in intellectual disability and related disorders. Nat. Rev. Genet. *17*, 9–18.
3. Vissers, L.E.L.M., de Ligt, J., Gilissen, C., Janssen, I., Steehouwer, M., de Vries, P., van Lier, B., Arts, P., Wieskamp, N., del Rosario, M., et al. (2010). A de novo paradigm for mental retardation. Nat. Genet. *42*, 1109–1112.
4. Deciphering Developmental Disorders Study (2017). Prevalence and architecture of de novo mutations in developmental disorders. Nature *542*, 433–438.
5. Miller, K.G. (2017). Keeping neuronal cargoes on the right track: New insights into regulators of axonal transport. Neuroscientist *23*, 232–250.
6. Iossifov, I., O'Roak, B.J., Sanders, S.J., Ronemus, M., Krumm, N., Levy, D., Stessman, H.A., Witherspoon, K.T., Vives, L., Patterson, K.E., et al. (2014). The contribution of de novo coding mutations to autism spectrum disorder. Nature *515*, 216–221.
7. Berger, S.I., Ciccone, C., Simon, K.L., Malicdan, M.C., Vilboux, T., Billington, C., Fischer, R., Introne, W.J., Gropman, A., Blancato, J.K., et al.; NISC Comparative Sequencing Program (2017). Exome analysis of Smith-Magenis-like syndrome cohort identifies de novo likely pathogenic variants. Hum. Genet. *136*, 409–420.
8. Sobreira, N., Schiettecatte, F., Valle, D., and Hamosh, A. (2015). GeneMatcher: A matching tool for connecting investigators with an interest in the same gene. Hum. Mutat. *36*, 928–930.
9. Lek, M., Karczewski, K.J., Minikel, E.V., Samocha, K.E., Banks, E., Fennell, T., O'Donnell-Luria, A.H., Ware, J.S., Hill, A.J., Cummings, B.B., et al.; Exome Aggregation Consortium (2016). Analysis of protein-coding genetic variation in 60,706 humans. Nature *536*, 285–291.
10. Samocha, K.E., Robinson, E.B., Sanders, S.J., Stevens, C., Sabo, A., McGrath, L.M., Kosmicki, J.A., Rehnström, K., Mallick, S., Kirby, A., et al. (2014). A framework for the interpretation of de novo mutation in human disease. Nat. Genet. *46*, 944–950.
11. Cockburn, J.J.B., Hesketh, S.J., Mulhair, P., Thomsen, M., O'Connell, M.J., and Way, M. (2018). Insights into Kinesin-1 Activation from the Crystal Structure of KLC2 Bound to JIP3 (Structure).
12. Xu, C., and Min, J. (2011). Structure and function of WD40 domain proteins. Protein Cell *2*, 202–214.
13. Guex, N., and Peitsch, M.C. (1997). SWISS-MODEL and the Swiss-PdbViewer: An environment for comparative protein modeling. Electrophoresis *18*, 2714–2723.
14. Sayle, R.A., and Milner-White, E.J. (1995). RASMOL: Biomolecular graphics for all. Trends Biochem. Sci. *20*, 374.
15. Edwards, S.L., Yu, S.C., Hoover, C.M., Phillips, B.C., Richmond, J.E., and Miller, K.G. (2013). An organelle gatekeeper function for Caenorhabditis elegans UNC-16 (JIP3) at the axon initial segment. Genetics *194*, 143–161.
16. Brown, H.M., Van Epps, H.A., Goncharov, A., Grant, B.D., and Jin, Y. (2009). The JIP3 scaffold protein UNC-16 regulates RAB-5 dependent membrane trafficking at C. elegans synapses. Dev. Neurobiol. *69*, 174–190.
17. Edwards, S.L., Morrison, L.M., Yorks, R.M., Hoover, C.M., Boominathan, S., and Miller, K.G. (2015). UNC-16 (JIP3) acts through synapse-assembly proteins to inhibit the active transport of cell soma organelles to caenorhabditis elegans motor neuron axons. Genetics *201*, 117–141.
18. Gowrishankar, S., Wu, Y., and Ferguson, S.M. (2017). Impaired JIP3-dependent axonal lysosome transport promotes amyloid plaque pathology. J. Cell Biol. *216*, 3291–3305.
19. Miller, K.G., Alfonso, A., Nguyen, M., Crowell, J.A., Johnson, C.D., and Rand, J.B. (1996). A genetic selection for Caenorhabditis elegans synaptic transmission mutants. Proc. Natl. Acad. Sci. USA *93*, 12593–12598.
20. Popp, M.W.-L., and Maquat, L.E. (2013). Organizing principles of mammalian nonsense-mediated mRNA decay. Annu. Rev. Genet. *47*, 139–165.
21. Stirnimann, C.U., Petsalaki, E., Russell, R.B., and Müller, C.W. (2010). WD40 proteins propel cellular networks. Trends Biochem. Sci. *35*, 565–574.
22. Perlson, E., Maday, S., Fu, M.-M., Moughamian, A.J., and Holzbaur, E.L.F. (2010). Retrograde axonal transport: Pathways to cell death? Trends Neurosci. *33*, 335–344.
23. Millecamps, S., and Julien, J.-P. (2013). Axonal transport deficits and neurodegenerative diseases. Nat. Rev. Neurosci. *14*, 161–176.
24. Schiavo, G., Greensmith, L., Hafezparast, M., and Fisher, E.M.C. (2013). Cytoplasmic dynein heavy chain: The servant of many masters. Trends Neurosci. *36*, 641–651.
25. Poirier, K., Lebrun, N., Broix, L., Tian, G., Saillour, Y., Boscheron, C., Parrini, E., Valence, S., Pierre, B.S., Oger, M., et al. (2013). Mutations in TUBG1, DYNC1H1, KIF5C and KIF2A cause malformations of cortical development and microcephaly. Nat. Genet. *45*, 639–647.
26. Di Donato, N., Timms, A.E., Aldinger, K.A., Mirzaa, G.M., Bennett, J.T., Collins, S., Olds, C., Mei, D., Chiari, S., Carvill, G., et al. (2018). Analysis of 17 genes detects mutations in 81% of 811 patients with lissencephaly. Genet. Med. *20*, 1354–1364.
27. Ravenscroft, G., Di Donato, N., Hahn, G., Davis, M.R., Craven, P.D., Poke, G., Neas, K.R., Neuhann, T.M., Dobyns, W.B., and Laing, N.G. (2016). Recurrent de novo BICD2 mutation associated with arthrogryposis multiplex congenita and bilateral perisylvian polymicrogyria. Neuromuscul. Disord. *26*, 744–748.
28. Huang, S.-H., Duan, S., Sun, T., Wang, J., Zhao, L., Geng, Z., Yan, J., Sun, H.-J., and Chen, Z.-Y. (2011). JIP3 mediates TrkB axonal anterograde transport and enhances BDNF signaling by directly bridging TrkB with kinesin-1. J. Neurosci. *31*, 10602–10614.
29. Magen, D., Ofir, A., Berger, L., Goldsher, D., Eran, A., Katib, N., Nijem, Y., Vlodavsky, E., Tzur, S., Behar, D.M., et al. (2015). Autosomal recessive lissencephaly with cerebellar hypoplasia is associated with a loss-of-function mutation in CDK5. Hum. Genet. *134*, 305–314.
30. Yeo, G.S.H., Connie Hung, C.-C., Rochford, J., Keogh, J., Gray, J., Sivaramakrishnan, S., O'Rahilly, S., and Farooqi, I.S. (2004). A de novo mutation affecting human TrkB associated with

severe obesity and developmental delay. Nat. Neurosci. *7*, 1187–1189.

31. Miller, K.A., Twigg, S.R.F., McGowan, S.J., Phipps, J.M., Fenwick, A.L., Johnson, D., Wall, S.A., Noons, P., Rees, K.E.M., Tidey, E.A., et al. (2017). Diagnostic value of exome and whole genome sequencing in craniosynostosis. J. Med. Genet. *54*, 260–268.
32. Hamdan, F.F., Myers, C.T., Cossette, P., Lemay, P., Spiegelman, D., Laporte, A.D., Nassif, C., Diallo, O., Monlong, J., Cadieux-Dion, M., et al.; Deciphering Developmental Disorders Study (2017). High rate of recurrent de novo mutations in developmental and epileptic encephalopathies. Am. J. Hum. Genet. *101*, 664–685.
33. Guerrini, R., and Parrini, E. (2010). Neuronal migration disorders. Neurobiol. Dis. *38*, 154–166.
34. Leventer, R.J., Jansen, A., Pilz, D.T., Stoodley, N., Marini, C., Dubeau, F., Malone, J., Mitchell, L.A., Mandelstam, S., Scheffer, I.E., et al. (2010). Clinical and imaging heterogeneity of polymicrogyria: A study of 328 patients. Brain *133*, 1415–1427.
35. Barkovich, A.J., Dobyns, W.B., and Guerrini, R. (2015). Malformations of cortical development and epilepsy. Cold Spring Harb. Perspect. Med. *5*, a022392.
36. Judkins, A.R., Martinez, D., Ferreira, P., Dobyns, W.B., and Golden, J.A. (2011). Polymicrogyria includes fusion of the molecular layer and decreased neuronal populations but normal cortical laminar organization. J. Neuropathol. Exp. Neurol. *70*, 438–443.
37. Ma, H., Yu, H., Li, T., Zhao, Y., Hou, M., Chen, Z., Wang, Y., and Sun, T. (2017). JIP3 regulates neuronal radial migration by mediating TrkB axonal anterograde transport in the developing cerebral cortex. Biochem. Biophys. Res. Commun. *485*, 790–795.
38. Moreno-De-Luca, A., Myers, S.M., Challman, T.D., Moreno-De-Luca, D., Evans, D.W., and Ledbetter, D.H. (2013). Developmental brain dysfunction: Revival and expansion of old concepts based on new genetic evidence. Lancet Neurol. *12*, 406–414.
39. Drerup, C.M., and Nechiporuk, A.V. (2013). JNK-interacting protein 3 mediates the retrograde transport of activated c-Jun N-terminal kinase and lysosomes. PLoS Genet. *9*, e1003303.
40. Sun, F., Zhu, C., Dixit, R., and Cavalli, V. (2011). Sunday Driver/JIP3 binds kinesin heavy chain directly and enhances its motility. EMBO J. *30*, 3416–3429.
41. Watt, D., Dixit, R., and Cavalli, V. (2015). JIP3 activates kinesin-1 motility to promote axon elongation. J. Biol. Chem. *290*, 15512–15525.
42. Sun, T., Yu, N., Zhai, L.-K., Li, N., Zhang, C., Zhou, L., Huang, Z., Jiang, X.-Y., Shen, Y., and Chen, Z.-Y. (2013). c-Jun NH2-terminal kinase (JNK)-interacting protein-3 (JIP3) regulates neuronal axon elongation in a kinesin- and JNK-dependent manner. J. Biol. Chem. *288*, 14531–14543.

The American Journal of Human Genetics, Volume *104*

Supplemental Data

De Novo Variants in *MAPK8IP3* Cause Intellectual Disability with Variable Brain Anomalies

Konrad Platzer, Heinrich Sticht, Stacey L. Edwards, William Allen, Kaitlin M. Angione, Maria T. Bonati, Campbell Brasington, Megan T. Cho, Laurie A. Demmer, Tzipora Falik-Zaccai, Candace N. Gamble, Yorck Hellenbroich, Maria Iascone, Fernando Kok, Sonal Mahida, Hanna Mandel, Thorsten Marquardt, Kirsty McWalter, Bianca Panis, Alexander Pepler, Hailey Pinz, Luiza Ramos, Deepali N. Shinde, Constance Smith-Hicks, Alexander P.A. Stegmann, Petra Stöbe, Constance T.R.M. Stumpel, Carolyn Wilson, Johannes R. Lemke, Nataliya Di Donato, Kenneth G. Miller, and Rami Jamra

Supplemental Tables

Table S1. Detailed clinical information of all individuals with causative *de novo* variants in *MAPK8IP3*

(Excel-file)

Table S2. *In silico* prediction of *de novo* missense variants and conservation of affected amino acids in *MAPK8IP3*

Chr16:g.	***De novo* variant**	**p.**	**REVEL** (Ioannidis *et al.*[1])	**CADD 1.4** (Kircher *et al.*[2])	**MutationTaster2** (Schwarz *et al.*[3])	**GERP** (Cooper *et al.*[4])	**Polyphen-2 v2.2.2r398** (Adzhubei *et al.*[5])	**SIFT** (Sim *et al.*[6])	**M-CAP** (Jagadeesh *et al.*[7])	**Conservation**[a] (up to indicated species)
1798706	c.1198G>A	p.Gly400Arg	0.560	32	DC	5.3	PD (1.000)	D (0.02)	PP (0.114)	high (zebrafish)
1810410	c.1331T>C	p.Leu444Pro	0.825	25.6	DC	5.47	PD (0.999)	D (0)	PP (0.799)	high (C. elegans)
1812389	c.1574G>A	p.Arg525Gln	0.521	28.2	DC	5.64	PD (0.998)	D (0)	PP (0.136)	high (C. elegans)
1812844	c.1732C>T	p.Arg578Cys	0.675	29.1	DC	4.42	PD (1.000)	D (0.02)	PP (0.284)	high (zebrafish)
1816769	c.2982C>G	p.His994Gln	0.379	23.3	DC	0.89	PD (0.998)	T (0.05)	PP (0.098)	high (fruitfly)
1817835	c.3436C>T	p.Arg1146Cys	0.472	25.3	DC	3.32	PD (1.000)	D (0)	PP (0.589)	high (C. elegans)

All genomic positions according to hg19, variant nomenclature corresponding to GenBank NM_015133.4.; D: deleterious; DC: disease causing; PD: probably damaging; PP: possibly pathogenic T: tolerated.

[a]Conservation was evaluated considering the following species: Homo sapiens, Pan troglodytes (chimp), Rattus norvegicus (rat), Mus musculus (mouse), Canis familiaris (dog), Ornithorhynchus anatinus (platypus), Gallus gallus (chicken), Xenopus tropicalis (frog), Tetraodon nigroviridis, Danio rerio (zebrafish), Drosophila melanogaster (fruitfly), Caenorhabditis elegans.

Supplemental Material and Methods

Exome Sequencing

Individuals 1 and 4. Parent-proband trio exome sequencing was performed using the IDT xGen Exome Research Panel v1.0. Bioinformatics filtering and data analysis were performed as previously described.[8] Candidate gene analysis and interpretation were performed as previously described.[9]

Individual 2. Whole exome analysis of the index individual was performed using the Nextera Exome capture on an Illumina HiSeq 4000. Bioinformatic analysis was carried out with an in-house developed pipeline relying on Burrows-Wheeler Alignment (BWA) and the Genome Analysis Toolkit (GATK). On target coverage was ≥ 10x in 96.0% with a median coverage of 97x.

Individuals 3, 6, 9, 10 and 12. Using genomic DNA from the proband and parents, the exonic regions and flanking splice junctions of the genome were captured using either the Clinical Research Exome kit (Agilent Technologies, Santa Clara, CA) for individual 3, individual 6 and individual 9 and the IDT xGen Exome Research Panel v1.0 for individual 10 and individual 12. Sequencing was done on an Illumina system with 100bp or greater paired-end reads. Reads were aligned to human genome build GRCh37/UCSC hg19, and analyzed for sequence variants using a custom-developed analysis tool. Additional sequencing technology and variant interpretation protocol has been previously described.[10]

Individuals 5 and 8. Agilent SureSelect All Exon V5 and V6 respectively were used for index and parents. Sequencing was performed using the Illumina HiSeq2500 and HiSeq400 respectively. Coverage on target was ≥ 10x for 98.78%, ≥ 20x for 97.31%, ≥ 30x for 94.84% and ≥ 10x for 96.76%, ≥ 20x for 95.57%, ≥ 30x for 93.25%, respectively. An analysis pipeline was used for both families as previously described.[11]

Individual 7. Trio exome sequencing was performed using the SureSelect All Human Version 6 (60 Mb) on a HiSeq 4000 platform. On target coverage was achieved ≥ 10x for 97.05% in the index individual. Analysis of the raw data was performed with the pipeline Varfeed (Limbus Medical Technologies) and variants were annotated and prioritized using the software Varvis (Limbus Medical Technologies).

Individual 11. Exome sequencing and variant calling using a parent-offspring trio approach was performed as described previously.[12] Briefly, the Agilent SureSelectXT Human All Exon v5 library prep kit was used (Agilent Technologies, Santa Clara, CA, USA). Sequencing was performed on an Illumina HiSeq 4000 instrument (Illumina, San Diego, CA, USA) with 101 bp paired-end reads at a median coverage of ×75 at the BGI Europe facilities (BGI, Kopenhagen, Denmark). Using Burrows-Wheeler Alignment (BWA) version 0.5.9-r16.14, sequence reads were aligned to the hg19 reference genome. Variants were subsequently called by the Genome Analysis Toolkit (GATK) unified genotyper, version 3.2-2. Annotation was performed using a custom built diagnostic annotation pipeline (DG.2.8).

Individual 13. Whole exome sequencing of index and parents was performed using the Agilent SureSelect Clinical research Exome v.2 on an Illumina NextSeq500 platform. An analysis pipeline was used as previously described.[13] Coverage on target for the index was ≥ 10x for 98.6% with a mean coverage of 200x.

C. elegans culture and strains

Worm culture and manipulation essentially followed previously described methods.[14–16] Briefly, culture media was modified NGM (referred to as NGM-LOB).[17] Prior studies defined the culture plate types “streak plates”, “locomotion plates”, “24-well plates”, and “96-well solid media culture plates”.[18–20] “96-well thrashing plates” were made similar to “96-well solid media culture plates”,[19] except the media volume per well was 305 µl, and the wells were not seeded with bacteria. “5 ml unseeded plates” were made by dispensing 5 mls of modified NGM into standard 60 mm petri plates,

allowing them to set overnight at room temperature lid-side-up, and storing unseeded at 4° until needed. Wild type was strain N2. Other *C. elegans* strains used in this study include KG2338 unc-16(ce483),[21] KG2430 ceIs56 [unc-129::CTNS-1-RFP, unc-129::nlp-21-Venus],[22] KG4192 unc-16(ce483); ceIs56,[23] and the 6 unc-16 mutants and their wild type revertant counterparts listed in Figure 3A in the main text.

Generation of unc-16 mutants and wild type revertants in C. elegans

With the exception of unc-16(ce856) and its mutationally-rescued counterpart, all mutations were generated using oligonucleotide-templated repair after producing targeted double strand breaks using the CRISPR-Cas9 system. All edits were targeted within 31 bp of the cut site. In addition to the targeted mutation, we introduced a silent mutation in the repair template that altered a restriction site, allowing us to screen for conversion by PCR followed by restriction digest. The oligo template contained ~50 bases of homology on each side of the mutated sequences. The oligo was ordered from Sigma at the 0.2 µmole scale with PAGE purification. The polarity of the oligonucleotide template was sense when the edit was left of the cut site and anti-sense when the edit was right of the cut site, as suggested by published guidelines.[24] Adult worms were injected as described.[25] Except where indicated (see below), the injected animals were N2 (wild type). F1 progeny containing the Co-CRISPR or co-transformation marker were allowed to lay eggs for 1-2 days before testing the F1's for the targeted edit using PCR and restriction digest. We chose homozygous lines not expressing the Co-CRISPR or co-transformation markers for analysis. The sequences around the edits were confirmed by PCR and sequencing.

To generate the unc-16(ce851) and unc-16(ce852) mutations, we used the oligonucleotide-templated co-conversion strategy ("Co-CRISPR"),[26] using dpy-10(cn64) as a co-conversion marker. We cloned the 20 bp Cas9 target sequence into the pJP118 gRNA expression cassette as previously described for cloning targeting sequences into pRB1017.[26] pJP118 is a modified version of the published pRB1017 plasmid.[26] It contains a modified sgRNA (F+E), with an extended Cas9 binding structure and removes a potential Pol III terminator by an A-U base pair flip. The injection mixture was pDD162 (Cas9

plasmid; 50 ng/µl),[27] pJA58 (dpy-10 gRNA plasmid; 25 ng/µl),[26] the experimental gRNA plasmid at 25 ng/µl, and the dpy-10(cn64) and experimental oligonucleotide repair templates (500 nM and 2400 nM, respectively). We injected ~60 wild type animals with this mixture and cloned 192 F1 rollers for each conversion. For unc-16(ce852), 6% of F1 rollers showed a restriction pattern consistent with the targeted edit, all of which were heterozygous. One of these lines was chosen and screened for homozygosity in the following generation. One homozygous line was chosen, and the sequence around the edit was confirmed by PCR and sequencing. For unc-16(ce851), 33% of F1 rollers showed a restriction pattern consistent with the targeted edit. One line was homozygous, indicating that edits occurred in both germlines.

To generate the mutationally-rescued (reverse-engineered) counterparts of unc-16(ce851) and unc-16(ce852), as well as the ce853, ce854, ce857 unc-16 alleles and their reverse-engineered counterparts, we used the high efficiency Co-CRISPR independent method described by Prior et al.[28] This method calls for injecting sgRNA-Cas9 complexes along with a myo-2::RFP co-transformation marker to select for progeny that incorporated the injection components. The complexes are made by combining the Alt-R® S.p. HiFi Cas9 Nuclease 3NLS (IDT) with a synthetic sgRNA with an optimized 80mer Synthego Scaffold (Sythego). The injection mixture was 300 mM KCl, 20 mM HEPES, pH 7.4, KG#381 (myo-2::RFP), 2.0 µM of the experimental Oligo repair template, 5 µM of the sgRNA, and 5 µM of the Cas9 enzyme. The injection mixture was incubated 30 min – 4 hr at 23° before injecting. Depending on the distance between the edit and the cut site, which ranged from 4 – 31 bp, we injected 60 – 100 animals and cloned 48 – 192 myo-2::RFP – positive F1's. An average of 35% of lines showed a restriction pattern consistent with the targeted edit (range 2.6% - 57%). 25% - 80% of positive F1's were homozygous, indicating that the conversions occurred in both germlines.

For unc-16(ce856), the targeted mutation site was 45 bp from the nearest cut site. We therefore generated this mutation in two steps. In the first step we deleted 108 bp between two cut sites that flanked the targeted edit site by co-injecting 2 sgRNAs with an oligonucleotide template homologous to the flanking regions to be joined, but that also inserted a 4 bp restriction site at the join. The restriction site insertion allowed us to use PCR and restriction digest to test whether the locus came

together by non-homologous end joining, which is prone to errors, or by homologous repair. It also allowed us to improve the protospacer for one of the cut sites that we would use in the second step. For the second step, we use GenePlus Economy (Genscript) to synthesize the 108 bp region to be re-inserted, including the targeted amino acid change, plus 35 – 37 bp homology arms. We amplified the DNA using eight 50 µl Q5 PCR reactions and concentrated the products to 818 ng/µl in 9 µl using the MinElute PCR purification kit (Qiagen). For both the first and second step, the injection mixtures were as described above for the high efficiency Co-CRISPR independent method. The second step injection mixture included 81 ng/µl of the PCR product. The first step used N2 (wild type as the host) and the second step used the strain containing the 108 bp deletion made in the first step. To mutationally rescue this strain back to the wild type sequence, we repeated these steps starting with the mutant strain, deleting the 108 bp region and replacing it with the wild type region.

Genetic crossing of C. elegans unc-16 mutations

For assaying lysosomes in axons, each mutation and its mutationally-rescued counterpart were crossed with the genomically integrated transgene ceIs56, which also expresses the ttx-3::RFP co-transformation marker. To cross the mutants with ceIs56, we crossed ceIs56 males with the mutant strain and, after 3d at 20°, cloned 5 ttx-3::RFP-positive L4-stage progeny to streak plates, grew them 4d at room temperature, and then cloned 14 ttx-3::RFP (red) putative homozygotes to streaks. After growing 4d at room temperature we tested all of these lines for homozygosity of the mutant using PCR and restriction digest. Homozygosity of ceIs56 was confirmed by checking for 100% ttx-3::RFP-positive animals in the chosen lines, final genotype: unc-16(ce____); ceIs56.

To cross the mutationally-rescued alleles with ceIs56, we crossed them through the original mutant background since the mutationally-rescued alleles could not be distinguished from wild type alleles by PCR and restriction digest. To do this, we made unc-16(ce____); ceIs56 males by heat shock and crossed them with hermaphrodites from the rescued strain. After 3d at 20°, we cloned 5 ttx-3::RFP-positive L4-stage progeny to streak plates, grew them 4d at room temperature, and then cloned 14 ttx-3::RFP (red) putative homozygotes to streaks. After growing 4d at room temperature we tested

all of these lines for homozygosity of the mutationally-rescued allele using PCR and sequencing (for ce863) or PCR and restriction digest (all other mutationally-rescued alleles). Homozygosity of ceIs56 was confirmed by checking for 100% ttx-3::RFP-positive animals in the chosen lines.

Quantitative fluorescence imaging of axonal lysosomes in C. elegans

Strain growth: Young adult progeny that had not previously been starved were grown for imaging as described.[23] ~55 young adults were selected and transferred to an unseeded plate immediately prior to mounting as described below.

Agarose pad slide production: Clean glass slides were produced as described.[23]

Mounting animals on agarose pad slides: We applied a 30 µl drop of 30 mg/ml BDM (2, 3-Butanedione monoxime; Sigma B0753) in M9 buffer onto a 24 X 30 mm coverslip. We then transferred the prepicked animals in one pick-full to the drop on the coverslip and incubated them for 10 min, placing the coverslip on a 1.5 cm square pad of folded paper towel tissue under a Petri plate lid. After the incubation, we removed ~19 µl of the solution using a P20 microinjection tip (Eppendorf 5242 956.003), leaving the worms behind in the remaining anesthetic, and inverted the coverslip onto a ~18-19 mm diameter 4% agarose pad that had been dried without its protective coverslip for the final 4 min of the incubation. We marked animal positions on the slide using a sharpie and imaged animals over the next 35 min.

Image acquisition and processing: We viewed animals using a Nikon Eclipse Ti-E inverted microscope equipped with a Nikon CFI Apo TIRF 100X/ 1.49 N.A. objective, a Nikon motorized high resolution z-drive, and a motorized filter turret containing GFP, YFP, and Texas Red filter cubes (Semrock). Our illumination source was a SOLA Light Engine LED source (Lumencor). We acquired images with an ORCA Flash 4.0 16-bit camera (Hamamatsu, Bridgewater, NJ) controlled by Metamorph v. 7.7. We controlled exposure times by using Metamorph to turn the LEDs on and off rather than using a shutter. We only collected images from animals with their dorsal surfaces facing the objective and used the “center quad” (center quadrant) mode of the camera. Z-series interval sizes (0.312 µm) and plane numbers (16) were the same for all strains. Exposure times were identical for different strains

in each experiment and chosen to collect at sub-saturating levels. Before imaging each strain, we measured the light power of the peak emission wavelength at the objective plane using an XR2100 power meter (Lumen Dynamics) and an XP750 objective plane light sensor (Lumen Dynamics) with the stage position set at a standard distance (z-position) from the objective. We then adjusted the percent power of the SOLA Light Engine to produce the targeted mW power for the experiment. We used AutoDeblur Gold CWF (Media Cybernetics) to deconvolve the image stacks using the Adaptive PSF blind method and 10 iterations at the low noise setting. After deconvolving, we used Metamorph to make maximum intensity projections of each image stack.

Quantifying Images: We used Metamorph 7.7 for all analysis and quantification. To quantify puncta per micron, we set a minimum pixel intensity threshold after viewing a series of images collected from unc-16(ce483) mutant dorsal axons. We then used the Threshold plug-in of Metamorph to highlight all pixels in the region that exceeded the threshold and counted the pixel clusters that exceeded this value, irrespective of the number of pixels in the cluster. We used the same threshold value in all strains throughout the experiment.

Producing Representative Images: After quantifying an image set we produced representative images for display by saving 8-bit versions of an image that was close to mean +/- standard error for the set. All representative images were scaled identically.

C. elegans locomotion assays

To grow animals for the assay, we transferred 13 L2 stage larvae to each of 4 Locomotion Plates and cultured the plates at 20° for 5 2/3 days to produce F1 young adults that had never been starved. The day before the assay, we adjusted the assay area temperature to 22.5 – 23.5° and set the following items in this area: one “96-well thrashing assay plate” (see “*C. elegans* Culture and Strains”), three “5 ml unseeded plate” (see “*C. elegans* Culture and Strains”), a 2L bottle of M9 with a 10 ml bottle top dispenser (set on 6 mls), a 100 ml bottle of M9, a count-down timer set on 3:00 min, a tally counter, and a 2.5 ml Combi-tip attached to a repeat pipetter and set on 75 µl. We made a “25 µl glass pipet

tip" by scoring and breaking off ~4 cm from the end of a Pasteur pipet, inserting a plastic gel-loading tip into the broken end, and securing the junction with Para film.

Prior to and during the assay, room thermostats were adjusted to keep the assay area temperature at 22.5° to 23.5°, as monitored by a CheckTemp digital thermometer kept near the stereoscope stage. To start the assay, one of the source plates was transferred from the 20° incubator to the assay area. A 2.5 ml Combi-tip on a repeat pipetter was used to fill the first 12 wells in row A of the 96-well Thrashing Plate with 75 µl of M9. The 5 ml Unseeded Plate was then filled with 12 mls of M9 using the bottle top dispenser. 12 young adult animals were transferred from the source plate into the 12 mls of M9 in the unseeded plate. We then used a P20 set on 25 ul and the 25 ul glass pipet tip to transfer those animals one at a time, in a full 25 µl of M9 to the first 12 wells of the assay plate. We then immediately focused on the animal in the first well, started a count-down timer, and used a tally counter to count swimming cycles for 3 min. We then recorded the counter value on the datasheet, reset the timer and tally counter, focused on the animal in the next well, started the timer, and counted for 3 min, etc. until we had assayed all 12 animals. We then repeated this for 5 more sets of 12 animals for 72 animals total, using a fresh 5 ml unseeded plate for every 24 animals assayed.

Supplemental References

1. Ioannidis, N.M., Rothstein, J.H., Pejaver, V., Middha, S., McDonnell, S.K., Baheti, S., Musolf, A., Li, Q., Holzinger, E. and Karyadi, D., et al. (2016). REVEL. An Ensemble Method for Predicting the Pathogenicity of Rare Missense Variants. American journal of human genetics *99,* 877–885.
2. Kircher, M., Witten, D.M., Jain, P., O'Roak, B.J., Cooper, G.M. and Shendure, J. (2014). A general framework for estimating the relative pathogenicity of human genetic variants. Nature genetics *46,* 310–315.
3. Schwarz, J.M., Cooper, D.N., Schuelke, M. and Seelow, D. (2014). MutationTaster2. Mutation prediction for the deep-sequencing age. Nature methods *11,* 361–362.
4. Cooper, G.M., Stone, E.A., Asimenos, G., Green, E.D., Batzoglou, S. and Sidow, A. (2005). Distribution and intensity of constraint in mammalian genomic sequence. Genome research *15,* 901–913.
5. Adzhubei, I.A., Schmidt, S., Peshkin, L., Ramensky, V.E., Gerasimova, A., Bork, P., Kondrashov, A.S. and Sunyaev, S.R. (2010). A method and server for predicting damaging missense mutations. Nature methods *7,* 248–249.
6. Sim, N.-L., Kumar, P., Hu, J., Henikoff, S., Schneider, G. and Ng, P.C. (2012). SIFT web server. Predicting effects of amino acid substitutions on proteins. Nucleic acids research *40,* W452-7.
7. Jagadeesh, K.A., Wenger, A.M., Berger, M.J., Guturu, H., Stenson, P.D., Cooper, D.N., Bernstein, J.A. and Bejerano, G. (2016). M-CAP eliminates a majority of variants of uncertain significance in clinical exomes at high sensitivity. Nature genetics *48,* 1581–1586.
8. Farwell, K.D., Shahmirzadi, L., El-Khechen, D., Powis, Z., Chao, E.C., Tippin Davis, B., Baxter, R.M., Zeng, W., Mroske, C. and Parra, M.C., et al. (2015). Enhanced utility of family-centered diagnostic exome sequencing with inheritance model-based analysis. Results from 500 unselected families with undiagnosed genetic conditions. Genetics in medicine : official journal of the American College of Medical Genetics *17,* 578–586.
9. Farwell Hagman, K.D., Shinde, D.N., Mroske, C., Smith, E., Radtke, K., Shahmirzadi, L., El-Khechen, D., Powis, Z., Chao, E.C. and Alcaraz, W.A., et al. (2017). Candidate-gene criteria for clinical reporting. Diagnostic exome sequencing identifies altered candidate genes among 8% of patients with undiagnosed diseases. Genetics in medicine : official journal of the American College of Medical Genetics *19,* 224–235.
10. Retterer, K., Juusola, J., Cho, M.T., Vitazka, P., Millan, F., Gibellini, F., Vertino-Bell, A., Smaoui, N., Neidich, J. and Monaghan, K.G., et al. (2016). Clinical application of whole-exome sequencing across clinical indications. Genetics in medicine : official journal of the American College of Medical Genetics *18,* 696–704.
11. Dohrn, M.F., Glöckle, N., Mulahasanovic, L., Heller, C., Mohr, J., Bauer, C., Riesch, E., Becker, A., Battke, F. and Hörtnagel, K., et al. (2017). Frequent genes in rare diseases. Panel-based next generation sequencing to disclose causal mutations in hereditary neuropathies. Journal of neurochemistry *143,* 507–522.
12. Ligt, J. de, Willemsen, M.H., van Bon, B.W.M., Kleefstra, T., Yntema, H.G., Kroes, T., Vulto-van Silfhout, A.T., Koolen, D.A., Vries, P. de and Gilissen, C., et al. (2012). Diagnostic exome sequencing in persons with severe intellectual disability. The New England journal of medicine *367,* 1921–1929.
13. Pezzani, L., Marchetti, D., Cereda, A., Caffi, L.G., Manara, O., Mamoli, D., Pezzoli, L., Lincesso, A.R., Perego, L. and Pellicioli, I., et al. (2018). Atypical presentation of pediatric BRAF RASopathy with acute encephalopathy. American journal of medical genetics. Part A, e40635.

14. Brenner, S. (1974). The genetics of Caenorhabditis elegans. Genetics *77,* 71–94.
15. Stiernagle, T. (2006). Maintenance of C. elegans. WormBook : the online review of C. elegans biology, 1–11.
16. Sulston, J. and Hodgkin, J. (1988). Methods. In The nematode Caenorhabditis elegans, W.B. Wood, ed. (Cold Spring Harbor, NY: Cold Spring Harbor Laboratory Press), pp. 596–597.
17. Hoover, C.M., Edwards, S.L., Yu, S.-c., Kittelmann, M., Richmond, J.E., Eimer, S., Yorks, R.M. and Miller, K.G. (2014). A novel CaM kinase II pathway controls the location of neuropeptide release from Caenorhabditis elegans motor neurons. Genetics *196,* 745–765.
18. Edwards, S.L., Charlie, N.K., Milfort, M.C., Brown, B.S., Gravlin, C.N., Knecht, J.E. and Miller, K.G. (2008). A novel molecular solution for ultraviolet light detection in Caenorhabditis elegans. PLoS biology *6,* e198.
19. Edwards, S.L., Yorks, R.M., Morrison, L.M., Hoover, C.M. and Miller, K.G. (2015). Synapse-Assembly Proteins Maintain Synaptic Vesicle Cluster Stability and Regulate Synaptic Vesicle Transport in Caenorhabditis elegans. Genetics *201,* 91–116.
20. Miller, K.G., Emerson, M.D. and Rand, J.B. (1999). Goalpha and diacylglycerol kinase negatively regulate the Gqalpha pathway in C. elegans. Neuron *24,* 323–333.
21. Edwards, S.L., Yu, S.-c., Hoover, C.M., Phillips, B.C., Richmond, J.E. and Miller, K.G. (2013). An organelle gatekeeper function for Caenorhabditis elegans UNC-16 (JIP3) at the axon initial segment. Genetics *194,* 143–161.
22. Edwards, S.L., Charlie, N.K., Richmond, J.E., Hegermann, J., Eimer, S. and Miller, K.G. (2009). Impaired dense core vesicle maturation in Caenorhabditis elegans mutants lacking Rab2. The Journal of cell biology *186,* 881–895.
23. Edwards, S.L., Morrison, L.M., Yorks, R.M., Hoover, C.M., Boominathan, S. and Miller, K.G. (2015). UNC-16 (JIP3) Acts Through Synapse-Assembly Proteins to Inhibit the Active Transport of Cell Soma Organelles to Caenorhabditis elegans Motor Neuron Axons. Genetics *201,* 117–141.
24. Paix, A., Folkmann, A., Goldman, D.H., Kulaga, H., Grzelak, M.J., Rasoloson, D., Paidemarry, S., Green, R., Reed, R.R. and Seydoux, G. (2017). Precision genome editing using synthesis-dependent repair of Cas9-induced DNA breaks. Proceedings of the National Academy of Sciences of the United States of America *114,* E10745-E10754.
25. Mello, C.C., Kramer, J.M., Stinchcomb, D. and Ambros, V. (1991). Efficient gene transfer in C.elegans. Extrachromosomal maintenance and integration of transforming sequences. The EMBO journal *10,* 3959–3970.
26. Arribere, J.A., Bell, R.T., Fu, B.X.H., Artiles, K.L., Hartman, P.S. and Fire, A.Z. (2014). Efficient marker-free recovery of custom genetic modifications with CRISPR/Cas9 in Caenorhabditis elegans. Genetics *198,* 837–846.
27. Dickinson, D.J., Ward, J.D., Reiner, D.J. and Goldstein, B. (2013). Engineering the Caenorhabditis elegans genome using Cas9-triggered homologous recombination. Nature methods *10,* 1028–1034.
28. Prior, H., Jawad, A.K., MacConnachie, L. and Beg, A.A. (2017). Highly Efficient, Rapid and Co-CRISPR-Independent Genome Editing in Caenorhabditis elegans. G3 (Bethesda, Md.) *7,* 3693–3698.